Separation Science and Technology
Publication details, including instructions for authors and subscription information:
http://www.informaworld.com/smpp/title~content=t713708471

Analysis on a Hydrophobic Hollow-Fiber Membrane Absorber and Experimental Observations of CO_2 Removal by Enhanced Absorption

Myung-Suk Chun[ab]; Kew-Ho Lee[a]
[a] MEMBRANES AND SEPARATION LABORATORY, KOREA RESEARCH INSTITUTE OF CHEMICAL TECHNOLOGY, SOUTH KOREA [b] Membranes Laboratory, Polymer Division, Korea Institute of Science & Technology, Seoul, South Korea

To cite this Article Chun, Myung-Suk and Lee, Kew-Ho(1997) 'Analysis on a Hydrophobic Hollow-Fiber Membrane Absorber and Experimental Observations of CO_2 Removal by Enhanced Absorption', Separation Science and Technology, 32: 15, 2445 — 2466
To link to this Article: DOI: 10.1080/01496399708000779
URL: http://dx.doi.org/10.1080/01496399708000779

SEPARATION SCIENCE AND TECHNOLOGY, 32(15), pp. 2445–2466, 1997

Analysis on a Hydrophobic Hollow-Fiber Membrane Absorber and Experimental Observations of CO_2 Removal by Enhanced Absorption

MYUNG-SUK CHUN* and KEW-HO LEE†
MEMBRANES AND SEPARATION LABORATORY
KOREA RESEARCH INSTITUTE OF CHEMICAL TECHNOLOGY
P.O. BOX 107, YUSUNG, TAEJON 305-606, SOUTH KOREA

ABSTRACT

In this paper an extended analysis on a hollow-fiber membrane absorber is conducted for CO_2 removal from flue gases. A rigorous model of gas–liquid mass transfer is developed on both narrow channels in and around the hollow fibers, including the gas absorption occurring from the reaction between CO_2 and aqueous K_2CO_3 absorbent. CO_2 concentration profiles can be obtained regardless of the placement of the flowing absorbent. Experimental observations of the CO_2 concentration in both the reject and permeate outlets compared with theoretical prediction allow us to understand the influence of flow rates of feed gas as well as absorbent on CO_2 absorption. For the flowing K_2CO_3 absorbent a kinetic constant can be chosen which will provide the best possible agreement between experiment and reactive model prediction. This fact emphasizes that the pseudofirst-order kinetic can be employed to describe the facilitation effect. The overall mass transfer coefficients were determined from the experimentally observed concentration changes. The CO_2 permeation flux was found to be enhanced as the K_2CO_3 concentration was increased, suggesting that CO_2 removal is entirely controlled by the reaction. The enhanced selectivity factor for CO_2/N_2, which decreases with increasing absorbent flow rate, reached as high as 1200 with 15 wt% K_2CO_3 absorbent.

Key Words. Hollow-fiber membrane absorber; Carbonates absorbent; Carbon dioxide removal; Mass transfer coefficient; Enhanced selectivity

* Current address: Membranes Laboratory, Polymer Division, Korea Institute of Science & Technology, Seoul 130-650, South Korea.
† To whom correspondence should be addressed. FAX: +82-42-861-4151.

INTRODUCTION

Large volume emission of CO_2 into the atmosphere caused by the mass consumption of fossil fuels is a main source of the global warming problem, including acid rain. Membrane-based gas absorption has recently attracted much attention as an efficient technique for CO_2 removal from flue gases (1–6). The amount of flue gases is generally large, and therefore a large contact area of the gas and liquid phases is required. In this respect a hollow-fiber membrane absorber (HFMA) offers significant advantages compared to such conventional absorbers as bubble columns and packed beds. In an HFMA a gas–liquid interfacial area is formed instead of the direct interaction found in conventional contactors. Another important advantage of an HFMA is its improved operational flexibility because no mutual influence is possible, while the operational flexibility in conventional absorbers is restricted by undesired phenomena like flooding and entrainment.

Many experimental studies pertaining to gas absorption with hollow-fiber membranes have been published in the literature. Qi and Cussler (7) studied the absorption of pure CO_2 in sodium hydroxide solutions using a hollow-fiber module with microporous polypropylene membranes. They also measured overall mass transfer coefficients for the absorption of a number of gases in aqueous solutions of NaOH or alkanolamines (8). Their results indicated that gas absorption with the gas phase flowing through and the liquid phase flowing around the fibers or vice versa could be achieved. Yang and Cussler (9) considered the influence of velocity on the mass transfer coefficient in their absorption experiments, and recognized a 10-fold increase in the gas absorption efficiency by using a hollow-fiber device compared to a conventional packed column. Kreulen et al. (10) also studied gas–liquid mass transfer in nonwetted microporous hollow-fibers with laminar flow, where a Graetz-Lévèque equation was used for the mass transfer through a single fiber.

Traditionally, there has been a great deal of effort in applying aqueous solutions of alkanolamines and carbonates as absorbents for CO_2 removal. Compared to a pure water absorbent, enhanced absorption incorporating a chemical reaction can obviously increase both the solubility and the CO_2 flux. The required absorbent flow rate is reduced as a consequence. Kreulen et al. (11) investigated the influence of a chemical reaction on mass transfer by simulation with a numerical model, and tested their model with experiments on CO_2 absorption in a hydroxide solution using hollow-fiber modules. It is clear that a higher selectivity can be obtained if the absorbent is reactive, preferably toward one particular species in a gas mixture. Many published data concerning facilitated behavior through an

absorbent are available for membrane-based CO_2 separation. Ever since the studies of Otto and Quinn (12) and Suchdeo and Schultz (13), aqueous K_2CO_3 solution has been widely used for CO_2 absorption. Besides an immobilized liquid membrane (ILM), both high flux and enhanced selectivity for CO_2/N_2 mixtures were obtained in a hollow-fiber containing liquid membrane (HFCLM) with 30 wt% K_2CO_3 solution (14). Results on enhanced gas absorption originating from facilitated CO_2 transport can also be found in the study of Guha et al. (15) employing an aqueous diethanolamine absorbent. Among recent results relative to the HFMA are those of Nii and Takeuchi (5) in which they describe the behavior of gas absorption utilizing alkalies and alkanolamines as absorbents.

CO_2 removal with HEMA is examined in the present work by initiating model analysis of enhanced gas absorption. In principle, the important advantage of a model approach is that it can be readily adapted to modules of various geometries, including any related operational variables. The relevant model for CO_2 absorption in both pure water and K_2CO_3 solution is developed, in which the available velocity profiles are employed on the tube and shell-sides of the fiber, respectively. The K_2CO_3 absorbent is chosen here with a view to furthering our forthcoming study of the additive effect on the carbonate solution. Instead of a complete consideration of its reaction scheme for describing the facilitation effect, a pseudofirst-order assumption for CO_2 absorption into 5 and 15 wt% K_2CO_3 solutions is applied. An unambiguous model prediction on the reaction effect in HFMA has not been addressed in previously reported work, possibly because of its awkward analysis. We carried out our experiments under the membrane condition of nonwetted pores, and then we compared the experimental observations of separation performance for CO_2/N_2 binary mixture with the theoretical results. The influence of the absorbent flow rate on the change of CO_2 concentration and the mass transfer characteristics, incorporating the separation performance, will receive particular emphasis in our discussion.

MODEL DEVELOPMENT

Our theoretical investigation on HFMA starts with the physical state of hollow-fiber membranes. The phase pressure conditions on each side of the membrane can be determined from the fact that the pores are filled with either absorbent liquid or gas, which are referred to as wetted and nonwetted, respectively. In the case of hydrophobic hollow-fibers with nonwetted pores, the liquid pressure has to be higher than that of the gas to prevent gas dispersion as bubbles in the liquid. Also, they do not permit passage of absorbent until a critical pressure is exceeded. The critical

pressure depends on the interfacial tension, the contact angle, and the size of openings in the pores. In this case the gas–liquid interface has the pore mouth on the liquid side. The gas–liquid mass transfer coefficients are generally much higher than the liquid-side mass transfer coefficient owing to the gas-filled pores. For example, polypropylene hydrophobic hollow-fibers of both Celgard X-10 and X-20 have a critical pressure of about 150 psi with a mean pore size of 0.03 μm. In hydrophilic hollow-fibers, the gas pressure has to be higher than the liquid pressure.

Mass Transfer Analysis

Both the gas and the absorbent can arbitrarily flow in either tube or shell-side. A fully developed velocity profile of the parabolic type is reasonably adopted for the tube-side. From a number of relevant analyses we know that the flow in the shell-side is more complex compared to the laminar tube-side flow. It is assumed that the fibers in the module are arranged in a regular pattern, i.e., an equilateral triangular pitch (16, 17). We can therefore expect a free surface to surround each fiber, which will allow formation of a flow channel in the shell-side as illustrated in Fig. 1. The free surface model for shell-side flow has been employed in previous works (3, 18). Hypothetical dashed lines for the shell-side of distance R_e can be defined from an outer radius of hollow-fiber r_o and a void fraction ϵ in a module, that is,

$$\left(\frac{r_o}{R_o}\right)^2 = 1 - \epsilon \tag{1}$$

where $R_o = r_o + R_e$. Owing to the symmetric property of the equilateral fiber array, a domain consisting of both a single fiber and its surrounding is the basis of our model.

The axial velocity profiles for tube and shell-sides with radial coordinates r_t and r_s can be determined as

$$v_{z,t}(r_t) = 2\bar{v}_t[1 - (r_t/r_i)^2] \tag{2}$$

$$v_{z,s}(r_s) = 2\bar{v}_s \times \Gamma(r_o, r_s, \epsilon) \tag{3}$$

where Γ is expressed as

$$\Gamma = \frac{[(R_o - r_s)/R_o]^2 - (1 - \epsilon) - 2\ln[(R_o - r_s)/r_o]}{\epsilon + 2 + (2/\epsilon)\ln(1 - \epsilon)} \tag{4}$$

Since the axial diffusion is negligible here (19), the general equation of the differential mass balance in cylindrical coordinates (r, z) is given as

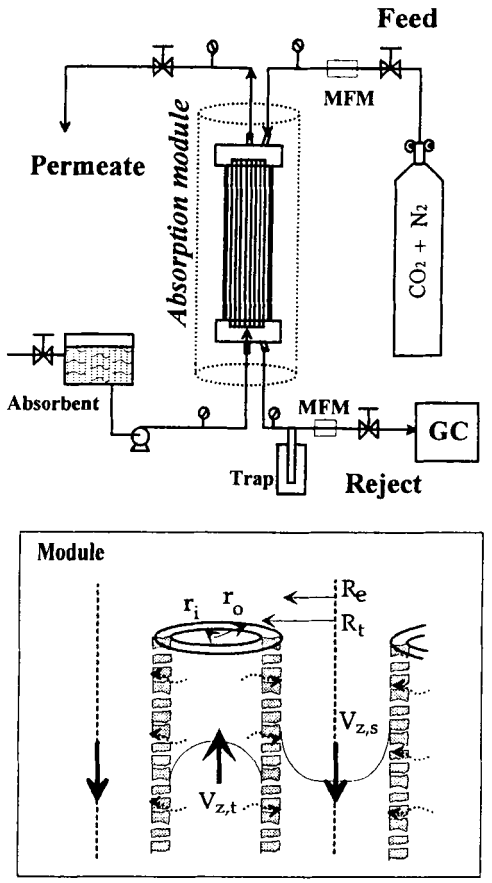

FIG. 1 Experimental setup of hollow-fiber membrane absorber and mass transfer in a gas/membrane/liquid system of nonwetted fibers.

$$v_{z,k}\frac{\partial C_{j,k}}{\partial z} = D_k\left[\frac{1}{r}\frac{\partial}{\partial r}\left(r\frac{\partial C_{j,k}}{\partial r}\right)\right] + (R_i) \tag{5}$$

where subscripts j and k denote the phase and the position, respectively. The $v_{z,k}$ corresponds to the prescribed axial velocity profile for the tube or shell-side. The reaction term R_i is the molar production rate of i-species associated with the facilitation effect. The concentration profile of the liquid phase can be estimated from Eq. (5) which completely describes

the diffusion, the convection, and the reaction in a medium. Mass transfer in the gas phase is similarly examined by Eq. (5); however, the reaction term need not be considered.

There are two possible flowing situations in the module of HFMA. One is that the liquid may flow through the tube-side of fibers whereas the gas flows through the shell-side. For the other case, the placements of each flow are located oppositely. In this case the problem of mass transfer can be solved by an identical procedure except for the conditions at the membrane interfaces (i.e., membrane–tube and membrane–shell interfaces).

We will first present the case for the liquid phase flowing in the tube-side. The concentration profile is symmetric at the centerline of the tube-side, and therefore satisfies boundary condition 1:

$$\left.\frac{\partial C_{l,t}}{\partial r_t}\right|_{r_t=0} = 0 \tag{6}$$

We remark here that all gases involved can be easily considered to be ideal gases, and so Henry's law is invoked. With the partition coefficient, namely the dimensionless Henry's law constant H, the following condition between gas and liquid phases is valid at the membrane–liquid interface ($r_t = r_i$) as

$$C_{g,m} = C_{l,t}/H \tag{7}$$

Flux continuity at this boundary is valid as follows:

$$D_m \frac{\partial C_{g,m}}{\partial r_t} = D_t \frac{\partial C_{l,t}}{\partial r_t} \tag{8}$$

in which one also needs to bear in mind the corresponding expression when the reaction effect exists. Boundary condition 2 can be imposed at this boundary, which takes the form

$$D_t \left.\frac{\partial C_{l,t}}{\partial r_t}\right|_{r_t=r_i} = \left[(C_{g,m})_{r_t=r_o} - \frac{(C_{l,t})_{r_t=r_i}}{H}\right] \frac{k_m(r_o - r_i)}{\ln(r_o/r_i)r_i} \tag{9}$$

where k_m is the mass transfer coefficient of the gas phase in the membrane (= D_m/membrane thickness), and $(r_o - r_i)/\ln(r_o/r_i)r_i$ is the shape factor (= S) based on the inside radius of tube r_i. The initial condition at the tube entrance ($z = 0$) is

$$C_{l,t}(r_t, 0) = C_{l,\text{inlet}} = 0 \tag{10}$$

Next, the gas phase on the shell-side has to be properly considered. At the centerline of the shell-side, boundary condition 1 is given by

$$\left.\frac{\partial C_{g,s}}{\partial r_s}\right|_{r_s=0} = 0 \tag{11}$$

The following conditions are valid at the membrane–gas interface ($r_s = R_e$):

$$C_{g,m} = C_{g,s} \tag{12}$$

$$D_m \frac{\partial C_{g,m}}{\partial r_s} = D_s \frac{\partial C_{g,s}}{\partial r_s} \tag{13}$$

Likewise, as was done above, boundary condition 2 can be readily written:

$$D_s \left.\frac{\partial C_{g,s}}{\partial r_s}\right|_{r_s=R_e} = \left[(C_{g,s})_{r_s=R_e} - \frac{(C_{l,t})_{r_s=R_t}}{H}\right] \frac{k_m(R_t - R_e)}{\ln(R_t/R_e)R_t} \tag{14}$$

The initial condition at the shell entrance ($z = z_L$) implies the feed gas concentration, yielding

$$C_{g,s}(r_s, z_L) = C_{g,\text{inlet}} \tag{15}$$

CO_2 Reaction with Pseudofirst Order in Carbonate Absorbents

The modeling of mass transfer coupled with the reaction becomes rather complicated due to an intricate reaction scheme contained in the usual rate equations. For the reaction term R_i of Eq. (5), we consider that CO_2 is absorbed in a solution of carbonate and bicarbonate. It reacts according to the following overall reaction (20, 21):

$$CO_2 + CO_3^{2-} + H_2O \rightleftarrows 2HCO_3^- \tag{16}$$

This reaction is trimolecular, and it is clearly made up in reality by a sequence of reactions, such as the hydration reactions and ionization reactions. Depending on the pH value, CO_2 may undergo two direct reactions in alkaline solution:

$$CO_2 + H_2O \xrightarrow{k_1} H^+ + HCO_3^- \qquad (pH > 8) \tag{17a}$$

$$CO_2 + OH^- \xrightarrow{k_2} HCO_3^- \qquad (pH > 10) \tag{17b}$$

and then the following instantaneous reactions occur:

$$CO_3^{2-} + H^+ \rightleftarrows HCO_3^- \tag{18a}$$

$$CO_3^{2-} + H_2O \rightleftarrows HCO_3^- + OH^- \tag{18b}$$

Any solution is not completely converted to bicarbonate, especially for the above pH range of K_2CO_3 solution. Therefore the reaction kinetics given by Eq. (16) may be expressed by

$$R_{CO_2} = (k_2 C_{OH^-}) C_{CO_2} = k_r C_{CO_2} \tag{19}$$

Equation (19) represents the pseudofirst-order kinetic equation adopted with the kinetic constant k_r. We note that the concentration of hydroxyl ions C_{OH^-} is determined by the buffer action of the equilibrium reaction of Eq. (18b), and it equals $K_f(C_{CO_3^{2-}}/C_{HCO_3^-})$. K_f is the ratio of the second dissociation constant of carbonic acid and the dissociation constant of water. Many experimental results reveal that the value of $(C_{CO_3^{2-}}/C_{HCO_3^-})$ ranges from 0.5 to 2 depending on the action at a given temperature. The values of k_2 and K_f found in the literature (20) depend somewhat on the temperature whereas the effect of ionic concentration is really unimportant. From the earlier reported data (20), it is found that the k_r value of 0.8 has been taken reasonably at 25°C with the $(C_{CO_3^{2-}}/C_{HCO_3^-})$ value of 1. Hence, the products of k_2 and K_f at 25 and 30°C are introduced here as 0.8 and 1.4, respectively.

Numerical Computation

Transport equations for the liquid and gas phases are combined with the corresponding equations for the tube and shell-sides of fibers, and solved simultaneously with the boundary conditions. For the liquid phase of the tube-side accompanied with the chemical reaction, the following dimensionless variables are introduced:

$$C^* = \frac{C_{l,t}}{C_{inlet}}, \qquad z^* = \frac{z k_r}{v_l}, \qquad r^* = \frac{r_t}{r_i}, \qquad \beta = \frac{D_t}{k_r r_i^2},$$

$$\theta = \frac{(C_{g,m})_{r_o}}{C_{inlet}}, \qquad Sh_t = \frac{r_i k_m S}{D_t} = \frac{D_m}{\ln(r_o/r_i) D_t} \tag{20}$$

β gives the ratio of the physical absorption flux and the chemically enhanced flux. The tube-side Sherwood number Sh_t is considered to be the ratio of mass transfer resistance in the tube-side to that in the membrane, and the shell-side Sherwood number also can be defined. Equation (5) and the appropriate boundary conditions of Eqs. (6) and (9) can be thus rewritten as

$$2(1 - r^{*2}) \frac{\partial C^*}{\partial z^*} = \beta \left[\frac{\partial^2 C^*}{\partial r^{*2}} + \frac{1}{r^*} \frac{\partial C^*}{\partial r^*} \right] + (C^*) \tag{21}$$

$$\text{IC:} \qquad C^* = 1 \qquad \text{at } r^* = r^* \tag{22}$$

$$\text{BC 1:} \quad \frac{\partial C^*}{\partial r^*} = 0 \qquad \text{at } r^* = 0 \tag{23}$$

$$\text{BC 2:} \quad \frac{\partial C^*}{\partial r^*} = \text{Sh}_t \left[\theta - \frac{C^*}{H}\right] \qquad \text{at } r^* = 1 \tag{24}$$

Equations (21)–(24) are solved by using a finite difference scheme of the Crank–Nicholson method (22, 23). The discretizations of the diffusion and convection terms result in the formation of a tridiagonal matrix in which an upward difference scheme for the convection term is used. The relevant equation for the gas phase is solved instantaneously. Since the shell-side flow is countercurrent to the tube-side flow, a downward difference scheme is adopted. The number of grid points is related with the computational accuracy and the CPU time. In most cases a grid of 20 × 1200 is chosen for our routine, and the computations are carried out with a MS-Fortran 5.1. Any results obtained should satisfy the mass balance of CO_2 in the module, which acts as an overall boundary condition on the HFMA simulation. The concentration field within the module can be clearly analyzed from the results of CO_2 concentration at any points of the axial and radial distances, from which we are able to predict subsequently the behavior of CO_2 absorption and mixing cup concentration.

EXPERIMENTS

Module Preparation and Setup

The microporous Celgard X-20 polypropylene hollow-fiber (Hoechst Celanese Co., USA) used here has an inner diameter of 400 μm, an outer diameter of 450 μm, a mean pore diameter of 0.03 μm, and a fiber wall porosity of 0.4. The symmetric pore structure of Celgard fiber can be seen from SEM analysis. As a fabrication procedure, the fibers were potted using Silant to prepare the fiber bundle, and then the fiber bundle was inserted into the constructed module. In order to obtain regular fiber packing, the fiber bundle was handled very carefully to avoid entanglement before potting. Epoxy resin was used to fill the annular space between the module shell and the two ends of the fiber bundle in which complete curing of the resin was carried out. The test module prepared in this study was of the cylindrical type with a contact length of 26 cm and an effective contact area (based on r_o) of 272.0 cm^2. The transparent membrane module allowed observation of any occurrences within the modules during the experiments.

The experimental setup for a HFMA is shown in Fig. 1. The gas composition of the CO_2/N_2 feed mixture was 23:77% with a purity of above

99.8%. The absorbent was pumped from a storage reservoir, and the flow rate was measured at the permeate outlet of the HFMA. The gas flow rate as controlled by accurate needle valves was essentially measured with a mass flowmeter (MKS instruments Inc., Model 247C-4-channel). Pressure changes in each stream were maintained by a pressure gauge. The module, kept in an isothermal condition, was equipped with a constant temperature bath, and our experiments were carried out at 25°C. A dry-ice trap at the reject outlet of the HFMA was used to measure accurately the reject flow rate with the gas phase. All data were obtained at steady state following sufficient operation time for stabilization, and any abnormal flow phenomena in the module, such as flooding or bubbling, were noted.

The gas compositions at the feed and reject sides were measured with an HP 5890A gas chromatograph using a thermal conductivity detector. A Chromosorb 102 column was used, and sampling was done continuously. A calibration curve was prepared to estimate the mole concentration of the sampled gas. The CO_2 concentrations in the liquid phase at the permeate side were measured with a CO_2 ion-selective electrode (Orion 9502BN) connected to a pH/ISE Meter (Orion Model 710A, Orion Research, MA, USA). The concentration measured by the electrode was cross-checked by comparison with the concentration estimated via the relation of mass balances for HFMA.

Absorbent Liquid

Aqueous K_2CO_3 solutions of 5 and 15 wt% were prepared as the carbonates absorbent. In order to carry out the model prediction on the enhanced absorption of CO_2, two physical parameters of diffusivity D and solubility coefficient σ are needed. These parameters, which vary according to the absorbent concentration, have a considerable effect on the permeate flux. The diffusivity of gas species in different concentrations of the K_2CO_3 solution can be estimated from the well-known Stokes–Einstein equation

$$D/D_w = \mu_w/\mu \tag{25}$$

where μ is the viscosity and subscript w means pure water. In principle, the solubility of a gas species in a nonreacting ionic solution can be estimated by the Setchenov equation (21, 24):

$$\log(\sigma/\sigma_w) = -E_i I \tag{26}$$

where the ion contribution constant E_i can be determined from the contributions of all ions in a solution. The ionic strength I ($= 1/2\Sigma m_i Z_i^2$) for K_2CO_3 solution can be estimated from $m(3 - y)$, in which y (=

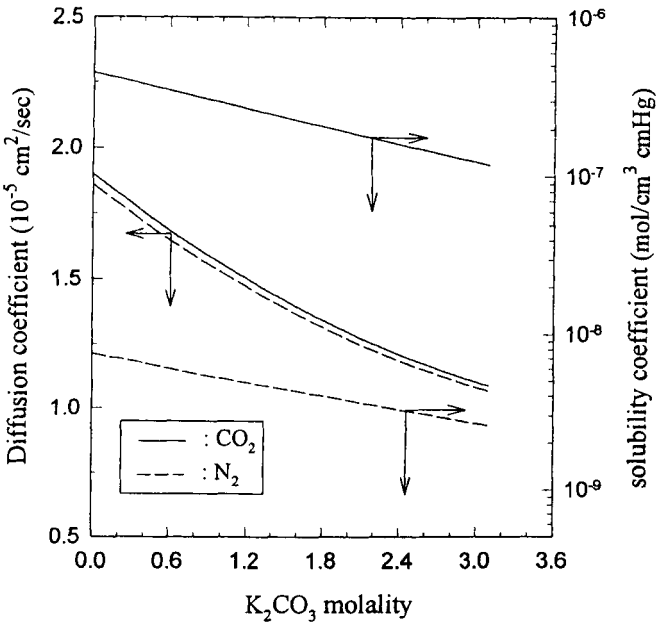

FIG. 2 Estimated solubility and diffusion coefficients according to K_2CO_3 molality.

$[HCO_3^-]/[K^+]$) ranges from 0.1 to 0.2. Finally, from the above relations we can obtain both the diffusivity and the solubility coefficient with a change of K_2CO_3 concentration as provided in Fig. 2. Note that a decrease of the N_2 solubility coefficient with the ionic strength of K_2CO_3 can be explained by the well-known salting-out effect. The solubility coefficient of CO_2 decreases like that of N_2 since Eq. (26) is adopted for the nonreacting case; however, the solubility is subsequently enhanced due to the facilitation effect in the presence of K_2CO_3.

RESULTS AND DISCUSSION

In order to simulate the numerical model, the diffusion coefficients of both the gas and membrane phases are required in addition to that of the liquid phase. The diffusion coefficient of the gas phase was evaluated from the Knudsen diffusivity, and the tortuosity for a nonwetted Celgard X-20 hollow-fiber is taken as 4.5. Table 1 lists the values used.

TABLE 1
The Diffusion Coefficients of Gases (at 25°C)[a]

	$D_s \times 10^2$ (cm²/s)	$D_m \times 10^3$ (cm²/s)
CO_2	3.8	3.4
N_2	4.7	4.2

[a] $D_m = D_s \times$ (porosity/tortuosity) (cf. Ref. 4).

Experimental Results Compared with Theoretical Prediction

Figure 3 shows the experimental results and subsequent comparison with theoretical prediction, where the operation mode of liquid flowing in the shell-side is taken. The dependency of the CO_2 concentration in the reject outlet with the gas flow rate is presented for different absorbent

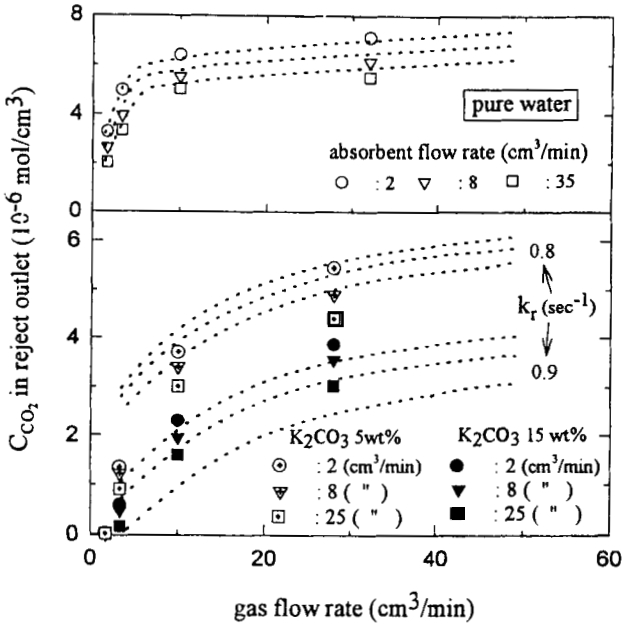

FIG. 3 Comparison between predicted and experimental CO_2 concentration in reject outlet as a function of gas flow rate for different absorbent flow rates. Upper and lower cases correspond to the water and reactive absorbents (K_2CO_3 5 and 15 wt%) with shell-side liquid flowing, respectively. Dotted curves indicate theoretical results.

flow rates. We point out that the result of liquid flowing in the tube-side corresponds to a lower flow rate for liquid flowing in the shell-side when the residence times of each phase involved with the flow velocities are considered. Further, the residence times at the gas–liquid interface, which may be closely related to the convective effect, determine the concentration profile of CO_2 in the module. The CO_2 concentration in the reject outlet increased with an increase in the gas flow rate, and it has a higher value as the absorbent flow rate decreases for the same gas flow rate. The computational accuracy is considerably reduced near the lower gas flow limit, mainly due to the steep concentration gradients in the region near the fiber wall. Although it can be improved somewhat if the grid density in the concentration field is better distributed, we do not present the numerical results for gas flow rates less than about 2 cm^3/min.

Figure 3 shows that as the K_2CO_3 concentration increases, the CO_2 concentration in the reject outlet is reduced accordingly. For theoretical predictions, computations have been conveniently performed with kinetic constants of 0.8 and 0.9 s^{-1}. While the theoretical prediction elegantly agreed with experiment in the case of pure water, the discrepancy between experiment and theory for K_2CO_3 absorbents is more apparent in the lower gas flow rate than in the higher gas flow rate. Even though good agreement does not hold over the whole range of gas flow rates, the experimental data lie in between the predicted results. This fact makes it straightforward to account for suitable assumptions for a pseudofirst-order kinetic from which the computational efforts are indeed reduced. As expected, the higher CO_2 absorption in K_2CO_3 absorbents compared to pure water is certainly induced by the facilitation effect in K_2CO_3 solutions. Our experiments ensure that the CO_2 concentration in the reject outlet is absorbed completely into 5 wt% K_2CO_3 absorbent at a gas flow rate of less than 1.7 cm^3/min. This flow rate may be used as the critical gas flow rate for complete CO_2 removal. Although additional data have not been provided in Fig. 3, this critical gas flow rate is increased with 15 wt% K_2CO_3 absorbent.

The dependency of the CO_2 concentration in the permeate outlet on the absorbent flow rate are presented in Fig. 4. The CO_2 concentration increases as the absorbent flow rate decreases, and the influence of the gas flow rate greatly increases at a lower absorbent flow rate. On the contrary, a decrease of CO_2 concentration in the permeate outlet cannot be observed at the high flow rate limit. We can determine the leveling-off absorbent flow rate where the CO_2 concentration decreases with a variation of less than about 1%. In this leveling-off region the CO_2 concentration in the permeate outlet evidently depends on the gas flow rate alone. Figure 4 shows that as the concentration of K_2CO_3 increases from 5 to 15

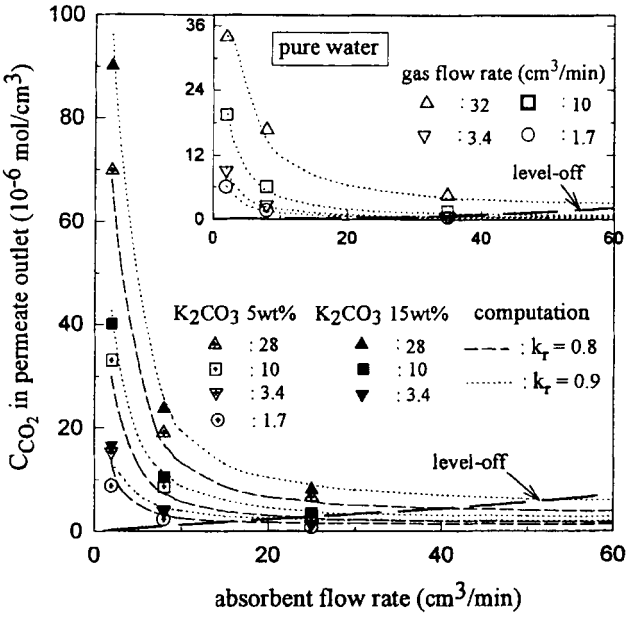

FIG. 4 Comparison between predicted and experimental CO_2 concentration in permeate outlet as a function of absorbent flow rate for different gas flow rates. Dotted and dashed curves indicate theoretical results.

wt%, the CO_2 concentration in the permeate outlet is obviously enhanced compared to pure water. Also, a large increase in the CO_2 concentration occurs in the lower absorbent flow rate.

Mass Transfer Enhancement

The experimentally detected concentration change from the feed inlet to the reject outlet is used to estimate the logarithmic-mean-based overall mass transfer coefficient K_{lm}, which is given as

$$K_{lm} = \frac{J}{\Delta C_{lm}} = \frac{Q_l}{A_c} \frac{C_{permeate}}{\Delta C_{lm}} \tag{27}$$

Here, J is the permeation flux, $C_{permeate}$ is the mean concentration of CO_2 in the permeate, Q_l is the absorbent flow rate, and A_c is the total gas–liquid contact area. The logarithmic mean concentration difference of gas species ΔC_{lm} can be estimated from the concentration differences at both sides of the HFMA module. The K_{lm} is related to the serial resistances

against mass transfer in the liquid, membrane, and gas phases, where it is well known that the gas-phase resistance is generally negligible. Figure 5 displays that overall mass transfer coefficient is proportional to an appropriate power of the absorbent flow rate, Q_l^n. The mass transfer is enhanced by the increased CO_2 absorption rate originating from the increased K_2CO_3 concentration, which offers practically a required absorber of smaller size. Figure 6 shows that exponent n obtained from the experimental results increases almost linearly as the gas flow rate increases, and also shows how n is enhanced with increasing K_2CO_3 concentration.

Experimental results are presented in Fig. 7 as a plot of Sherwood number ($= 2R_e K_{lm}/D_s$) versus Graetz number for the shell-side ($= \pi R_e^2 \bar{v}_s / LD_s$). For liquid flow around fibers in a triangular array, the correlation derived by Miyatake and Iwashita (25) can be applied. Our results obtained with pure water are somewhat lower than this correlation. This deviation may be attributed to an inevitable irregularity on the packing of our test module as well as the possibly of variations of shell-side flow in wide channels. We have found a similar deviation in behavior in the literature (10). However, there is a clear trend in Fig. 7 that Sh increases with

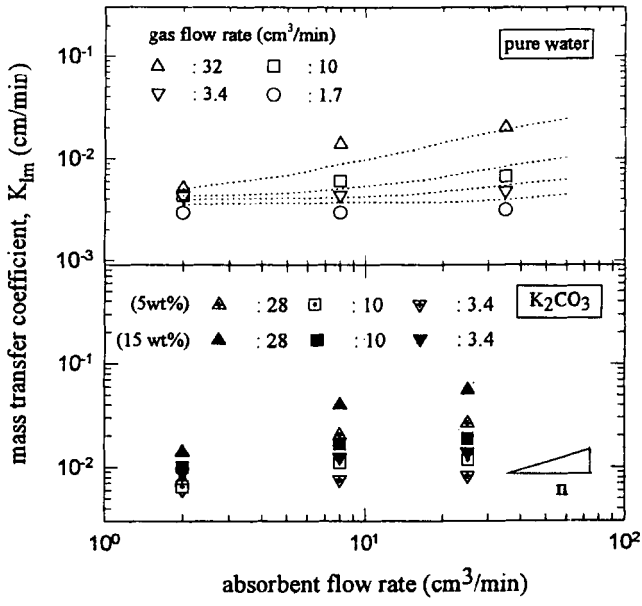

FIG. 5 The plot of mass transfer coefficient versus absorbent flow rate for different gas flow rates. Dotted curves in the upper panel indicate theoretical results.

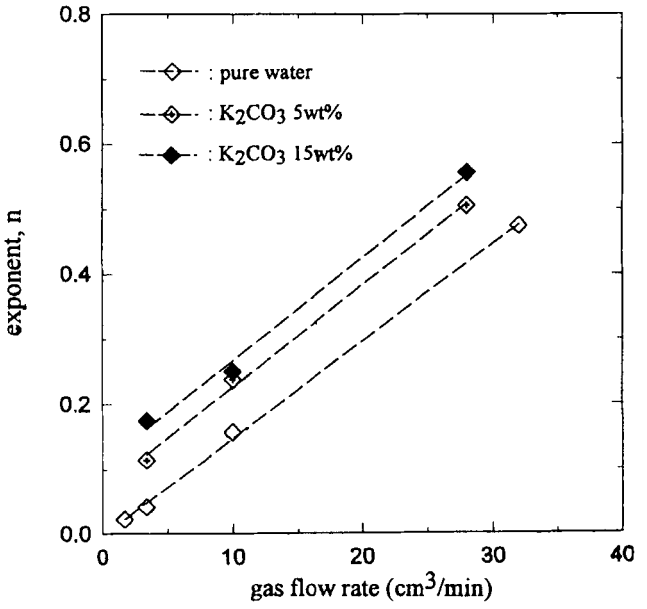

FIG. 6 Variation in exponent n versus gas flow rate profiles with different absorbents.

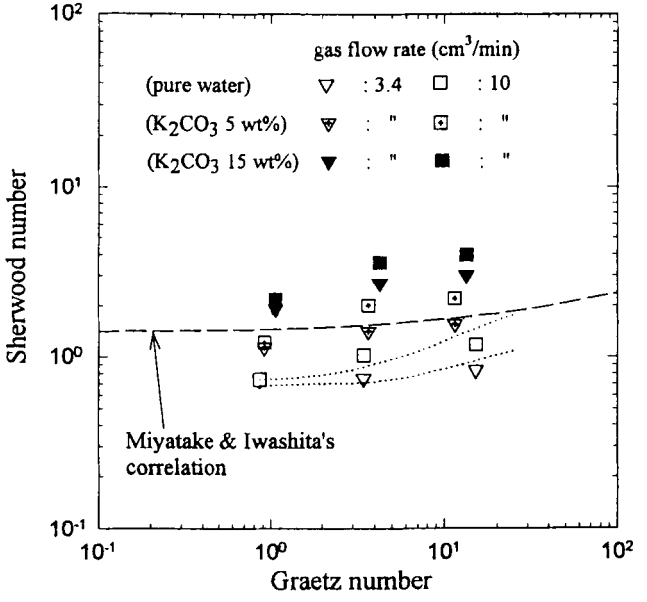

FIG. 7 The plot of Sh versus Gz for the results of enhanced CO_2 absorption in HFMA. Dotted curves indicate theoretical results for pure water with gas flow rates of 3.4 and 10 cm^3/min.

an increase in K_2CO_3 concentration. Although our module may not be attractive for practical application owing to its low packing fraction, it certainly makes a case for examining the basic features of the HFMA. Further experiments with some kinds of practical modules are necessary as future research.

Enhanced CO_2 Absorption: Flux and Selectivity Factor

As shown in Fig. 8, the permeation fluxes of both CO_2 and N_2 increase as the absorbent flow rate increases. CO_2 permeation flux is enhanced with increasing K_2CO_3 concentration. The behavior of enhanced CO_2 absorption was already revealed in the results of CO_2 concentration in the permeate outlet as shown in Fig. 4. Contrary to what is observed in CO_2, the N_2 permeation flux decreases with the K_2CO_3 concentration. In this regard, we earlier explored the salting-out effect by providing Fig. 2. We can readily expect that the flux behavior of both CO_2 and N_2 with K_2CO_3 concentration, acting in opposite directions, will give rise to enhancement of the selectivity factor.

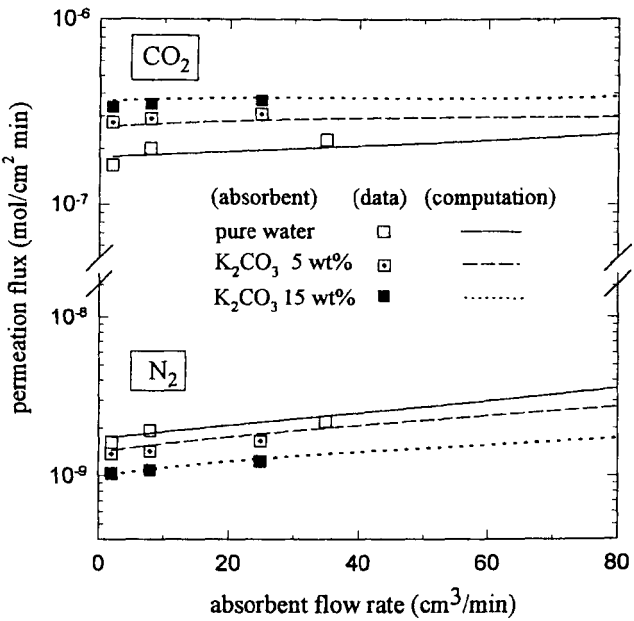

FIG. 8 The permeation flux of both CO_2 and N_2 for different absorbent flow rates of pure water and K_2CO_3 (5 and 15 wt%). The gas flow rate is 10 cm^3/min.

The enhanced absorption behavior in HFMA is explicitly concerned with its ability for CO_2 removal, which can be justified by estimation of the selectivity factor for gas mixtures. Figure 9(a) shows that the selectivity factor of CO_2/N_2 decreases gradually with an increase of the absorbent flow rate. For the 15 wt% K_2CO_3 absorbent, the highest selectivity factor achieved at an infinite lower flow rate can be approximately 1200, which is more than 3 times higher than that of pure water, which is about 350. It is difficult to determine a further increase of the selectivity factor by experiments since for K_2CO_3 concentrations above 15 wt% the detection of the N_2 concentration in the reject outlet by using the gas chromatographic technique does not permit proper measurement. Selectivity enhancement due to chemical absorption is shown in Fig. 9(b), where this enhancement decreases somewhat with an increase of the absorbent flow rate. The results obtained in this work indicate that the removal of acid gases through the use of HFMA is an emerging technology.

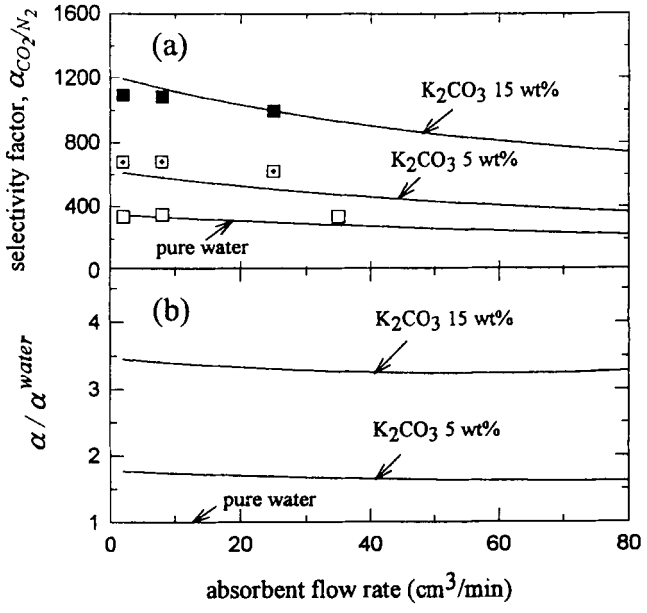

FIG. 9 (a) Selectivity factor for CO_2/N_2 with the variations of absorbent flow rate, and (b) the corresponding enhanced behavior for K_2CO_3 concentration in absorbents.

CONCLUDING REMARKS

The CO_2 concentration profile in the HFMA module has been explicitly predicted by the finite difference scheme on a rigorous model of gas–liquid mass transfer combined with chemical reaction. A completely accurate model is not easy to develop fully; however, a pseudofirst-order kinetic for the CO_2 reaction with K_2CO_3 absorbent was applied as a suitable assumption. Our experimental investigations using a test module included measurements of CO_2 concentration in both the reject and permeate outlets with changes in the flow rates of the absorbent as well as of the feed gas. The experimental results have been compared with the theoretical prediction for which the relevant physical parameters were taken from literature.

In the HFMA the CO_2 concentration in the reject outlet increased with an increase of the gas flow rate, whereas the CO_2 concentration in the permeate outlet decreased with an increase of the absorbent flow rate. Enhanced CO_2 removal can be observed from the increase of CO_2 concentration in the permeate outlet as the K_2CO_3 concentration increases, which is clearly attributable to the facilitation effect of the carbonate absorbent. This contribution, which incorporates the salting-out effect, enhances both the permeation flux and the selectivity factor compared with nonreactive pure water. Mass transfer enhancement due to chemical absorption was also examined. This work contributes fundamentally to the development of a practical system aimed at CO_2 separation and recovery.

NOMENCLATURE

A_c	total gas–liquid contact area of HFMA (cm^2)
C	concentration (mol/cm^3)
ΔC_{lm}	logarithmic mean concentration difference (mol/cm^3)
D	diffusion coefficient (cm^2/s)
E_i	ion contribution constant (cm^3/mol)
Gz	Graetz number (—)
H	dimensionless Henry's law constant (—)
I	ionic strength (mol/cm^3)
J	permeation flux [$mol/(cm^2 \cdot min)$]
K_f	ratio of the dissociation constant of carbonic acid and of water (mol/cm^3)
K_{lm}	logarithmic mean overall mass transfer coefficient (cm/s)
k_m	mass transfer coefficient in membrane phase (cm/s)
k_r	kinetic constant of reaction (1/s)
k_1	first-order rate constant of Eq. (17a) (1/s)

k_2 rate constant of Eq. (17b) (cm^3/mol)
L gas–liquid contact length (cm)
m molality [mol/cm^3]
Q_1 absorbent flow rate (cm^3/min)
R reaction term [mol/(cm^3·s)]
R_e equivalent inner radius of shell-side channel (cm)
R_o $= r_o + R_e$ (cm)
R_t outer radius of shell-side channel (cm)
r radial coordinate position (—)
r_i inner radius of hollow-fiber (cm)
r_o outer radius of hollow-fiber (cm)
Sh Sherwood number (—)
v flow velocity (cm/s)
Z_i valency of ith species (—)
z axial coordinate position (—)

Greek Letters

α selectivity factor (—)
β dimensionless variable (—)
Γ geometric factor in shell-side velocity profile of Eq. (3) (—)
ϵ void fraction of module (—)
θ dimensionless variable (—)
μ viscosity [g/(cm·s)]
σ solubility coefficient [mol/(cm^3·cmHg)]

Subscripts

g gas phase
i species
j phase
k position
l liquid phase
m membrane-side
s shell-side
t tube-side
w pure water

Superscripts

* dimensionless
– mean

ACKNOWLEDGMENTS

This investigation was supported by a Highly Advanced National Research Project (NG-1022) from the Korea Ministry of Environments, and the authors acknowledge the financial support.

REFERENCES

1. H. Matsumoto, H. Kitamura, T. Kamata, N. Nishikawa, and M. Ishibashi, "Fundamental Study of CO_2 Removal from Thermal Power Plant Flue Gas by Hollow-Fiber Gas-Liquid Contactor," *Kagaku Kogaku Ronbunshu*, *18*, 804 (1992).
2. A. B. Shelekhen and I. N. Beckman, "Gas Separation Processes in Membrane Absorber," *J. Membr. Sci.*, *73*, 73 (1992).
3. S. Karoor and K. K. Sirkar, "Gas Absorption Studies in Microporous Hollow Fiber Membrane Modules," *I&EC Res.*, *32*, 674 (1993).
4. H. Kreulen, C. A. Smolders, G. F. Versteeg, and W. P. M. van Swaaij, "Determination of Mass Transfer Rates in Wetted and Non-Wetted Microporous Membranes," *Chem. Eng. Sci.*, *48*, 2093 (1993).
5. S. Nii and H. Takeuchi, "Removal of CO_2 and/or SO_2 from Gas Streams by a Membrane Absorption Method," *Gas Sep. Purif.*, *8*, 107 (1994).
6. H. Matsumoto, H. Kitamura, T. Kamata, M. Ishibashi, H. Ota, and N. Akutsu, "Effect of Membrane Properties of Microporous Hollow-Fiber Gas-Liquid Contactor on CO_2 Removal from Thermal Power Plant Flue Gas," *J. Chem. Eng. Jpn.*, *28*, 125 (1995).
7. Z. Qi and E. L. Cussler, "Microporous Hollow Fibers for Gas Absorption, Part I: Mass Transfer in the Liquid," *J. Membr. Sci.*, *23*, 321 (1985).
8. Z. Qi and E. L. Cussler, "Microporous Hollow Fibers for Gas Absorption, Part II: Mass Transfer across the Membranes," *Ibid.*, *23*, 333 (1985).
9. M.-C. Yang and E. L. Cussler, "Designing Hollow-Fiber Contactors," *AIChE J.*, *32*, 1910 (1986).
10. H. Kreulen, C. A. Smolders, G. F. Versteeg, and W. P. M. van Swaaij, "Microporous Hollow Fiber Membrane Modules as Gas-Liquid Contactors. Part 1. Physical Mass Transfer Processes. A Specific Application: Mass Transfer in Highly Viscous Liquids," *J. Membr. Sci.*, *78*, 197 (1993).
11. H. Kreulen, C. A. Smolders, G. F. Versteeg, and W. P. M. van Swaaij, "Microporous Hollow Fiber Membrane Modules as Gas-Liquid Contactors. Part 2. Mass Transfer with Chemical Reaction," *Ibid.*, *78*, 217 (1993).
12. N. C. Otto and J. A. Quinn, "The Facilitated Transport of Carbon Dioxide through Bicarbonate Solutions," *Chem. Eng. Sci.*, *26*, 949 (1971).
13. S. R. Suchdeo and J. S. Schultz, "The Permeability of Gases through Reacting Solutions: The Carbon Dioxide-Bicarbonate Membrane System," *Ibid.*, *29*, 13 (1974).
14. S. Majumdar, A. K. Guha, and K. K. Sirkar, "A New Liquid Membrane Technique for Gas Separation," *AIChE J.*, *34*, 1135 (1988).
15. A. K. Guha, S. Majumdar, and K. K. Sirkar, "Facilitated Transport of CO_2 through an Immobilized Liquid Membrane of Aqueous Diethanolamine," *I&EC Res.*, *29*, 2093 (1990).
16. I. Noda and C. C. Gryte, "Mass Transfer in Regular Arrays of Hollow Fibers in Countercurrent Dialysis," *AIChE J.*, *25*, 113 (1979).

17. C. K. S. Jones, R. Y. K. Yang, and E. T. White, "A Novel Hollow-Fiber Reactor with Reversible Immobilization of Lactase," *Ibid.*, *34*, 293 (1988).
18. J. Happel, "Viscous Flow Relative to Arrays of Cylinders," *Ibid.*, *5*, 174 (1959).
19. E. L. Cussler, *Diffusion: Mass Transfer in Fluid Systems*, Cambridge University Press, New York, NY, 1984.
20. G. Astarita, *Mass Transfer with Chemical Reaction*, Elsevier, New York, NY, 1967.
21. G. Astarita, D. W. Savage, and A. Bisio, *Gas Treating with Chemical Solvents*, Wiley, New York, NY, 1983.
22. J. H. Ferziger, *Numerical Methods for Engineering Application*, Wiley, New York, NY, 1981.
23. C. F. Gerald and P. O. Wheatley, *Applied Numerical Analysis*, 4th ed., Addison-Wesley, 1992.
24. J. A. Dean (Ed.), *Lange's Handbook of Chemistry*, 14th ed., McGraw-Hill, New York, NY, 1992.
25. O. Miyatake and H. Iwashita, "Laminar-Flow Heat Transfer to a Fluid Flowing Axially between Cylinders with a Uniform Surface Temperature," *Int. J. Heat Mass Transfer*, *33*, 417 (1990).

Received by editor June 13, 1997
Revision received February 1997